Sensors & Diagnostics

PAPER

View Article Online
View Journal | View Issue

Cite this: *Sens. Diagn.*, 2023, **2**, 382

The design of anti-fouling and anti-hydrolysis cyclic peptides for accurate electrochemical antigen testing in human blood†

Rui Han, Wenjie Hou, Yang Li, Min Chen, Caifeng Ding* and Xiliang Luo *

Antigen testing is an effective methodology for COVID-19 disease screening, and the receptor-binding domain of the SARS-CoV-2 spike glycoprotein (RBD) is recognized as a key biomarker for the diagnosis, treatment, and vaccination of COVID-19. However, the diagnosis of RBD directly in human biofluids remains a serious challenge owing to severe biological fouling in real samples. Herein, a sensitive electrochemical biosensor capable of detecting the RBD antigen in human blood was constructed based on a self-designed cyclic peptide. This cyclic peptide was designed to have good antifouling properties to resist nonspecific adsorption of proteins, *etc.* in blood, and the cyclic structure of the peptide was able to resist enzymatic hydrolysis by certain enzymes in blood, enhancing the stability of the peptide as well as the peptide-based biosensor. Compared with conventional linear peptides, the cyclic peptide possessed better antifouling properties and a much stronger anti-enzymatic hydrolysis ability. The electrochemical biosensor based on the cyclic peptide was capable of sensitively assaying RBD in the concentration range from 1.0 pg mL^{-1} to 100.0 ng mL^{-1}, with a limit of detection of just 0.45 pg mL^{-1}. Moreover, the biosensor was able to quantitatively detect RBD in real samples, and the results were more reliable than those measured with ELISA kits, especially in human blood with higher concentrations. This strategy of designing cyclic peptides for the construction of antifouling biosensors offered a new method for clinical detection of viral antigens in complex biological media like human blood.

Received 25th November 2022,
Accepted 15th December 2022

DOI: 10.1039/d2sd00213b

rsc.li/sensors

1. Introduction

COVID-19, caused by a novel coronavirus (SARS-CoV-2), has resulted in more than 6 million deaths and affected more than 400 million people worldwide, as well as presenting critical challenges to the global healthcare systems.[1,2] So far, there have been two main approaches for the disease screening of COVID-19: (1) real-time fluorescence (RT-PCR) for the novel coronavirus nucleic acid[3] and (2) novel coronavirus-specific antibody screening by serological analysis.[4] In general, nucleic acid testing, as the "gold standard", is the preferred method for the detection of novel coronaviruses due to the most reliable and accurate steps in detecting coronavirus in COVID-19 infected patients.[5] Besides nucleic acid testing, antibody testing is generally used as a supplemental analysis for patients with a novel coronavirus or in conjunction with nucleic acid testing in the diagnosis of suspected cases.[6] For example, patients infected with a novel coronavirus have a greater increase in specific IgG antibodies within the serum compared to normal individuals.[7] Nevertheless, it takes a period of latency for the virus to enter the body before antibodies (IgM and IgG) are produced, and therefore antibody testing cannot be used for early diagnosis.

Notably, antigen testing, as a new potential approach for disease screening of COVID-19, can directly detect the constituent proteins of the virus, as antigens are produced before antibodies, making it more suitable for early screening.[8] Convenient, rapid, and relatively inexpensive antigen detection methods for COVID-19 have been developed, such as lateral immunochromatography[9] and enzyme-linked immunosorbent assay (ELISA).[10] In contrast, biosensing devices developed with electrochemical technology provide the advantages of rapid response and high sensitivity in antigen detection.[11–13] However, antigen testing may generate false-positive or false-negative results owing to biofouling and nonspecific protein adsorption in complex biological matrices, and it is generally less accurate.[14–16]

The modification of sensing interfaces with antifouling materials is regarded as an effective means to address

Key Laboratory of Optic-electric Sensing and Analytical Chemistry for Life Science, MOE, Shandong Key Laboratory of Biochemical Analysis, College of Chemistry and Molecular Engineering, Qingdao University of Science and Technology, Qingdao 266042, China. E-mail: caifengding@qust.edu.cn, xiliangluo@qust.edu.cn; Fax: +8653284022681; Tel: +86 53284022860

† Electronic supplementary information (ESI) available. See DOI: https://doi.org/10.1039/d2sd00213b

biofouling issues.[17,18] Peptides have raised considerable interest due to their good biocompatibility, structural diversity, and ease of synthesis and further modification.[15] Many specifically designed peptides have been reported to have good antifouling properties.[19–22] Among them, linear peptides have been the most widely and intensively studied, and for the synthesis of linear peptides, both liquid-phase and solid-phase methods have been well established.[23] Although many linear peptides have good biological activity and stability *in vitro*, they get degraded quickly after contact with biological media due to the presence of various protein hydrolases (such as endopeptidase and exopeptidase), leading to a loss of activity.[19] In addition, the conformational flexibility of linear peptides makes them not easy to be self-assembled in an orderly manner at the functional interface.[24,25]

In order to obtain peptides with enhanced stability, numerous methods of peptide modification have been reported, including the formation of cyclic peptides.[26] Such macrocyclic molecules have a well-defined and rigid conformation, which can keep the structure stable. In addition, the absence of free amino- and carboxyl-termini within the molecules of cyclic peptides makes them much less sensitive to aminopeptidase and carboxypeptidase.[27,28] Generally speaking, the metabolic stability of cyclic peptides is much higher than that of linear peptides.[29–31] In view of the advantages of cyclic peptides, the synthesis, biological evaluation, and application of cyclic peptides have received increasing attention in recent years.[32,33]

Herein, a cyclic peptide with antifouling and anti-hydrolysis functions was designed, and used for biosensor fabrication, in order to detect the SARS-CoV-2 spike glycoprotein receptor-binding domain (RBD) as a pathogenic antigen expressed by a novel coronavirus. The conducting polymer poly(3,4-ethylenedioxythiophene) (PEDOT), a conductive material with good stability and biocompatibility,[19,20] and a gold nanoparticle (AuNP) modified electrode were used as a substrate for the immobilization of the cyclic peptide and angiotensin-converting enzyme 2 (ACE2) in sequence, to fabricate an antifouling electrochemical biosensor for the detection of RBD (Scheme 1). Compared with linear peptides, the designed cyclic peptide exhibited enhanced resistance to biofouling and enzymatic hydrolysis, ensuring that the fabricated biosensor has high stability and accuracy for RBD detection in serum and exhibiting promising potential for COVID-19 diagnosis.

2. Experimental section

2.1. Materials

The cyclic peptide (cPep) c(CEKEKEKEK) and the linear peptides NH2-CEKEKEKEK-COOH (lPep1) and NH2-CPPPPEKEKEKEK-COOH (lPep2) were synthesized by the Bankpeptide Biological Technology Co. Ltd. (Hefei, China). 3,4-Ethylenedioxythiophene (EDOT), 1-ethyl-3-dimethylaminopropyl carbodiimide (EDC) and *N*-hydroxysuccinimide (NHS) were purchased from Aladdin (Shanghai, China). Fluorescein isothiocyanate labeled BSA (FITC-BSA) was purchased from Adamas-Beta Reagent (Shanghai, China). SARS-CoV-2 spike glycoprotein receptor binding domain (RBD), angiotensin-converting enzyme 2 (ACE2), aminopeptidase (Ap), and carboxypeptidase B (cPB) were purchased from Sangon Biotech (Shanghai, China). Immunoglobulin G (IgG), immunoglobulin M (IgM), human epidermal growth factor receptor 2 (HER2), carbohydrate antigen 15-3 (CA15-3), carbohydrate antigen 12-5 (CA12-5), carcinoembryonic antigen (CEA), alpha fetoprotein (AFP) and other supplements were provided by Solarbio (Beijing, China). *Escherichia coli* (*E. coli*), purchased from Nanjing LeZhen Biotech Co., Ltd., (Nanjing, China), was used for all experiments. An RBD ELISA kit was purchased from Sino Biological, Inc. (Beijing, China). Human blood samples from healthy individuals were provided by Qingdao Eighth People's

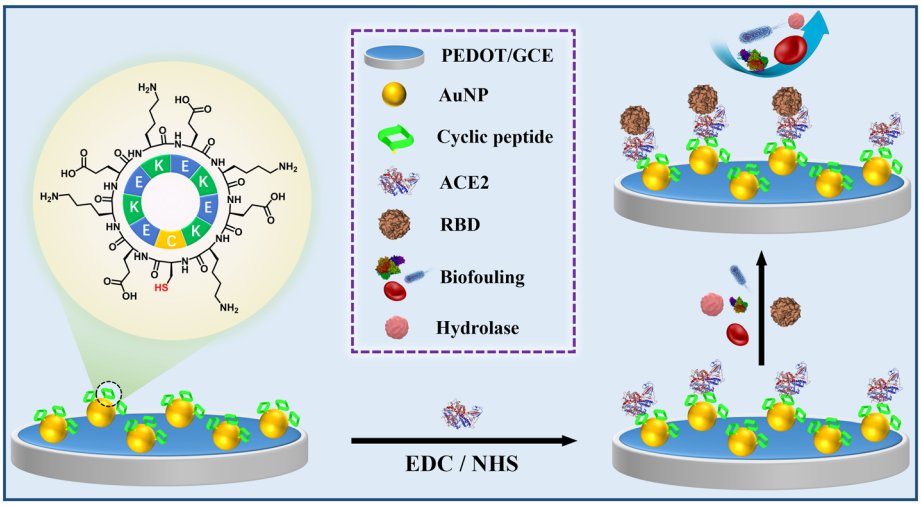

Scheme 1 The assembly procedure of the electrochemical cyclic peptide-based biosensor for the assay of RBD.

Hospital (Qingdao, China). All sample preparations were approved by the institution and followed hospital usage guidelines with relevant regulations and standard procedures. Informed consents were obtained from the human participants of this study. Ultrapure water with a resistivity of over 18.0 MΩ cm was purified from Millipore's (Bedford, USA) Milli-Q system.

2.2. Peptide synthesis and characterization

cPep was synthesized by the Fmoc solid-phase method followed by cyclization in the solution and purified using reversed phase high-performance liquid chromatography (RP-HPLC). Linear peptides were synthesized using the same technique. The molecular structural formulas of all peptides are exhibited in Fig. S1.† The structure details of the cyclic peptide and linear peptides were characterized utilizing ^{1}H-NMR spectroscopy and circular dichroism (CD) spectra.

2.3. Molecular dynamics simulations

All atom molecular dynamics (MD) simulations were used to explore the properties of the linear peptides and cyclic peptide. All MD simulations were performed using the molecular dynamics package GROMACS 2020.6,[34,35] with the Amber_99SB-ILDN force field and the TIP3P water model.[36] Na^+ and Cl^- were added to neutralize the charge and maintain the ionic strength of the physiological state (0.15 M NaCl). The particle-mesh Ewald (PME) method was used to evaluate electrostatic interactions, where a cutoff of 1.2 nm was used. Minimization was performed using the conjugate gradient method and then the equilibrium of temperature and pressure was then obtained under the NVT and NPT ensembles, respectively. Subsequently, the MD simulations were performed to collect data with a time step of 2 fs.

2.4. Enzymatic hydrolysis experiment and protein adsorption tests

Single protein adsorption tests were performed by incubating in FITC-BSA solution (10.0 mg mL^{-1}) at 37 °C for 24 h, to observe protein adsorption on the surfaces modified with the linear peptides and cyclic peptide. Different modified surfaces were immersed in aminopeptidase and carboxypeptidase B enzyme solutions (1.0 mg mL^{-1} in 10.0 mM PBS, pH 7.4, respectively) and stored for 12 h, followed by incubating in FITC-BSA solution under the same conditions again for the single protein adsorption tests.

2.5. Fabrication of the cyclic peptide-based biosensor

Glassy carbon electrodes (GCEs) were polished with Al_2O_3 powder and then cleaned using an ultrasonic bath with water and ethanol, respectively. Then, the GCEs were steeped in 7.4 mM EDOT solution containing 0.5 mg mL^{-1} $LiClO_4$ and electropolymerization was carried out at a constant potential of 1.0 V for 20 s, to prepare PEDOT/GCE. After rinsing and nitrogen blow-drying, the modified electrode was placed in 5.0 mM $HAuCl_4$ solution containing 0.5 mM KNO_3, and gold nanoparticles (AuNPs) were electrodeposited on the electrode using cyclic voltammetry (CV).[21] Subsequently, the prepared electrode (AuNP/PEDOT/GCE) was immersed in 0.2 mM cyclic peptide solution and kept shaking overnight at room temperature, to self-assemble the peptide onto the electrode surface (through the gold–sulfur bonds between the cysteine of the cyclic peptide and AuNPs). Afterwards, cPep/AuNP/PEDOT/GCE was soaked in PBS (pH 7.0) containing 0.1 mM EDC-NHS for 30 min, and then rinsed with PBS and immersed in 1.0 μM ACE2 solution to immobilize ACE2 onto the electrode surface (ACE2/cPep/AuNP/PEDOT/GCE). DPV signals of the biosensor were recorded for the detection of different concentrations of RBD with electrochemical cells with phosphate buffered saline (PBS, 10.0 mM, pH 7.4) containing 0.1 M KCl and 5.0 mM $[Fe(CN)_6]^{3-/4-}$.

2.6. Cell and bacteria adsorption experiments

Collected fresh blood was added with EDTA to prevent clotting, and stored at 2–8 °C for no more than 24 h for a cell adhesion assay. Different modified electrodes were placed in blood diluted to 25% (V/V) with PBS (containing 0.9% NaCl) for 24 h, and the adsorption of blood cells to the electrode surfaces was observed and recorded by laser confocal microscopy. Subsequently, a medium inoculated with *E. coli* was incubated at 37 °C for 24 h to generate a sufficient density of bacterial colonies and then the bacteria were collected to configure the bacterial solution with a concentration of 10^6 CFU mL^{-1}. Then, the modified electrodes were placed in the bacterial solution for 24 h, and the adsorption of *E. coli* stained with SYBR Green I on the electrode surfaces was observed and recorded by laser confocal microscopy.

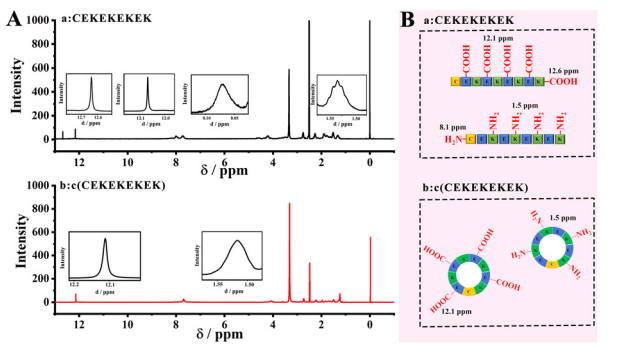

Fig. 1 (A) ^{1}H-NMR spectra of (a) the linear peptide lPep1 and (b) the cyclic peptide cPep in $CDCl_3$. Insets show peak shifts of $-NH_2$ and –COOH for side-chain or terminal residues of peptides. (B) Schematic structures of (a) lPep1 and (b) cPep with relevant ^{1}H-NMR shifts of $-NH_2$ and –COOH from the side chain or terminal of peptides.

3. Results and discussion

3.1. Peptide characterization

^{1}H NMR was performed to verify that the peptide was successfully cyclized. As shown in Fig. 1A, the ^{1}H-NMR peaks of the linear peptide lPep1 appeared at δ = 8.1 ppm and δ = 12.6 ppm, indicating the presence of terminal amino- and carboxyl-groups, which were absent in the ^{1}H NMR spectrum of cPep due to the cyclization of peptides (Fig. 1B). In addition, ^{1}H-NMR peaks at δ = 1.5 ppm and δ = 12.1 ppm were present in both peptides, due to the presence of the free amino group of the side-chain from lysine (K) and the free carboxyl group of the side-chain from glutamic acid (E).

The zeta potentials of different peptide solutions were measured, and similar electrical distributions near 0.0 mV were obtained for both the aqueous solutions of cPep and lPep1 (Fig. S2†). The zeta potential analysis indicated that the cyclization of the peptide does not significantly change the electrical properties, and the cyclic peptide remains electrically neutral.

The antifouling properties of various peptide-modified electrodes were tested in 10.0 mg mL^{-1} FITC-BSA solution. Compared with the peptide-free surface (Fig. S3A†), the peptide-modified surfaces exhibited much lower protein adsorption, due to the antifouling ability of the peptides. In addition, the cyclic peptide cPep modified surface showed the best antifouling properties (Fig. S3D†), and lPep2 was superior to lPep1, owing to the structural differences of the peptides.

The secondary structures of peptides were further studied by CD, as shown in Fig. S4.† The CD spectrum of lPep2 features a negative absorption band near 200 nm and a relatively weak positive absorption band near 225 nm, with an α-helical structure composed of polyproline (–PPPP–), which has been proven to be beneficial for improving the antifouling properties owing to the rigid structure of lPep2 and the higher packaging density on the surface.[22] In contrast, the CD spectrum of lPep1 exhibited a typical disordered structure with low ellipticity above 215 nm and negative bands at lower than 200 nm. Notably, the CD spectrum of cPep showed a negative peak at a wavelength of about 220 nm, which represents a typical peak of β-hairpin/β-helical super-secondary structure, and this kind of conformation is of high stability.[37]

To assess the stability of peptides, Gibbs free energy landscape maps of the cyclic peptide (cPep) and linear peptide (lPep1) were obtained by molecular dynamics simulations using first (PC1) and second (PC2) eigenvector projections of peptides, respectively.[38] The dark blue regions in the plots indicate the low energy states with highly stable peptide conformations, while the red regions indicate the high energy states and unstable peptide conformations. As seen in Fig. 2A and B, the cyclic peptide exhibited a smaller and more concentrated global free energy region, indicating a highly stable conformational state compared with the linear peptide (Fig. 2C and D).

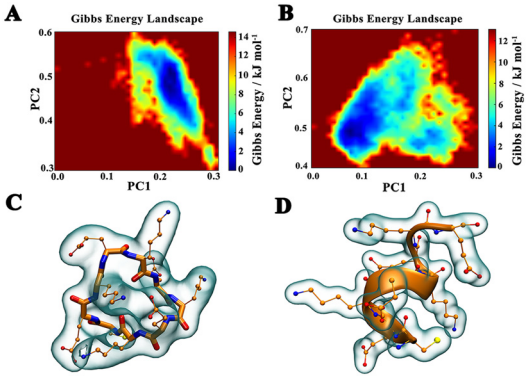

Fig. 2 The Gibbs free energy landscape plots obtained by MD simulations for cPep (A) and lPep1 (B). Representative structures of the lowest energy states of cPep (C) and lPep1 (D).

3.2. Enzymatic hydrolysis of peptides

To examine the enzymatic hydrolysis properties of different peptides, various electrodes modified with different peptides (cPep, lPep1 and lPep2) were soaked in solutions of 0.1 mg mL^{-1} cPB and Ap for 12 h, respectively. The FITC-BSA protein adsorption levels were recorded before and after enzymatic hydrolysis treatments using a laser confocal microscope. As shown in Fig. S5 and S6,† a large amount of BSA was adsorbed on the linear peptide (lPep1 and lPep2) modified electrodes after cPB and Ap treatment, respectively, exhibiting the extremely poor resistance to enzymatic degradation of the two linear peptides. However, the cPep modified electrodes displayed no obvious change after cPB and Ap treatment, demonstrating the high stability of the cyclic peptide in the presence of protein hydrolases.

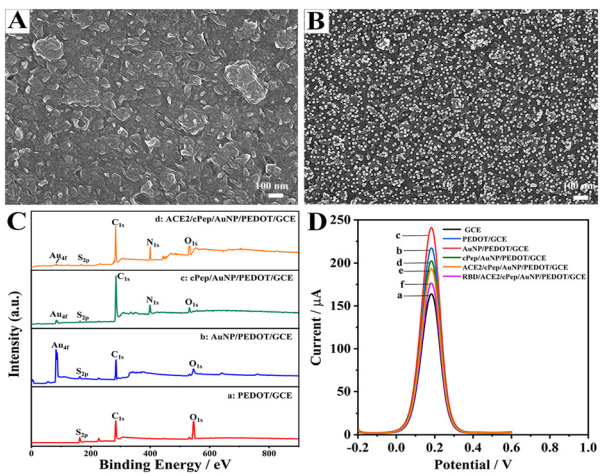

Fig. 3 SEM images of PEDOT/GCE (A) and AuNPs/PEDOT/GCE (B). (C) XPS spectra of (a) PEDOT, (b) AuNP/PEDOT, (c) cPep/AuNP/PEDOT and (d) ACE2/cPep/AuNP/PEDOT modified electrode surfaces. (D) DPV curves of various electrodes in a solution containing 0.1 M KCl and 5.0 mM $[Fe(CN)_6]^{4-/3-}$: (a) GCE, (b) PEDOT/GCE, (c) AuNP/PEDOT/GCE, (d) cPep/AuNP/PEDOT/GCE, (e) ACE2/cPep/AuNP/PEDOT/GCE and (f) RBD/ACE2/cPep/AuNP/PEDOT/GCE.

3.3. Fabrication of the electrochemical biosensor

Electrodeposition with PEDOT and AuNPs increases the conductivity and sensitivity of the modified electrodes. SEM images of PEDOT/GCE and AuNP/PEDOT/GCE are shown in Fig. 3A and B. The rough surface of electrodeposited PEDOT can be clearly observed, and AuNPs with a diameter of about 20 nm were uniformly distributed on the PEDOT surface.

The hydrophilicity of different modified electrode surfaces was characterized by contact angle experiments (Fig. S7†). After electrodeposition of PEDOT and AuNPs on GCE, the contact angles were 53.13 ± 2.84° and 75.01 ± 4.24°, respectively. After the self-assembly of the cyclic peptide, the contact angle declined to 14.5 ± 1.47°, indicating that the cyclic peptide was able to remarkably improve the hydrophilic performance of the electrode surface.

Fig. 3C shows the XPS spectra of electrodes after different modification steps. Firstly, the appearance of sulfur S2p (164.2 eV), carbon C1s (284.8 eV) and oxygen O1s (533.0 eV) as characteristic elements of PEDOT proved the successful PEDOT electrodeposition.[39] Following the electrodeposition of AuNPs, the characteristic peak of Au4f was observed to appear at 84.03 eV.[19] When cPep was self-assembled onto the electrode, the N1s peak appeared at 399.71 eV.[21] Finally, after the immobilization of ACE2, a significant increase in the intensity of the N1s peak was observed. Thus, it was experimentally verified that the electrodeposition of PEDOT and AuNPs and the immobilization of cyclic peptides and ACE2 were appropriately implemented.

The assembly process of the biosensor was recorded by DPV (Fig. 3D). The DPV peak current of the bare GCE was around 160 μA, and after the electrodeposition of PEDOT and AuNPs, the peak current increased significantly, which is attributed to the electrical conductivity and large electroactive surface area of PEDOT and AuNPs. However, after the self-assembly of cPep and immobilization of ACE2, as well as the binding of the target RBD, significant decreases of the DPV peak currents were observed, owing to the poor electrical conductivity of these biomolecules which impeded the electron transfer of the electrode surfaces.

3.4. Characterization of the antifouling properties

Accurate diagnosis directly in body fluids (*e.g.*, blood) is paramount and therefore requires that the biosensor exhibits antifouling properties in complex biological media.[19] Hence, the antifouling abilities of various modified electrodes in complex human blood were evaluated (Fig. S8†). The electrodes modified with antifouling peptides (cPep, lPep1 and lPep2) showed less signal suppressions compared with AuNP/PEDOT/GCE after soaking in different concentrations of human blood for 30 min. Interestingly, the superior antifouling ability of cPep/AuNP/PEDOT/GCE was presented in human blood, and the signal change rate was only 3.10% (lPep1: 8.84% and lPep2: 5.91%) in 25% healthy human blood and 6.17% (lPep1: 13.43% and lPep2: 10.10%) in whole blood. This result indicated that the great antifouling performance of the designed cyclic peptide was superior to that of the linear peptides. Just as expected, the signal suppression rates of the biosensor (ACE2/cPep/AuNP/PEDOT/GCE) were only 4.13% in 25% healthy human blood and 8.15% in whole blood, demonstrating the unique antifouling capability of the biosensors constructed using cyclic peptides.

Long-term application is essential for a sensing device, which requires the device to be able to maintain signal stability over a long period of time.[40–42] Hence, the long-term biofouling resistance was also examined for various modified electrodes in human blood (Fig. 4A). Over a monitoring period of 20 days, the linear peptide (lPep1 and lPep2) modified electrodes displayed a significant decrease in DPV signal after incubation in 25% blood, with change rates of 33.44% and 26.78%, respectively. However, the cyclic peptide modified electrodes exhibited a much lower rate of signal change (9.76%). These results indicated that the cyclic peptide possessed better long-term antifouling performance than the linear peptides, attributed to the fact that the cyclic peptide can resist enzymatic hydrolysis in human blood. In addition, as illustrated in Fig. 4B, the cyclic peptide-based biosensor also maintained good stability and biofouling resistance over 20 days, and the DPV signal retention rate exceeds 85%. Therefore, these results indicated that the biosensor constructed using the cyclic peptide possessed good long-term antifouling performance.

The effect of blood cells in human blood and external bacteria on the biosensor was also investigated by incubating the biosensors with *E. coli* (10^6 CFU mL^{-1}) and 25% human blood for 24 h. As shown in Fig. 4C and D, numerous *E. coli* cells were adsorbed on AuNP/PEDOT/GCE, while few *E. coli* cells were observed on the biosensor surface, indicating that the designed cyclic peptide possessed an outstanding antifouling capability and effectively prevented bacteria adhesion. Similarly, a high number of erythrocytes were

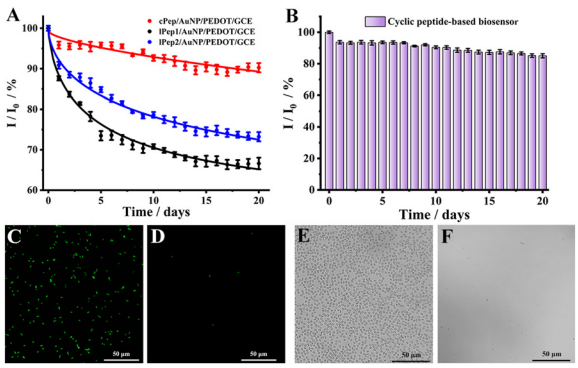

Fig. 4 (A) Long-term stability of the electrodes modified with different peptides in 25% human blood. (B) Biosensor stability when stored in 25% human blood. Each bar represents the mean standard deviation across three replicate measurements. Confocal fluorescence microscopy images of the peptide-free surface (C) and biosensor surface (D) after incubation with *E. coli* (10^6 CFU mL^{-1}). Bright-field images of the peptide-free surface (E) and biosensor surface (F) after incubation in 25% human blood captured under a confocal fluorescence microscope.

observed on the peptide-free electrode surface, while few erythrocytes were observed on the biosensor surface (Fig. 4E and F). These experimental results directly verified the good antifouling performance of the cyclic peptide-based biosensor in the presence of a large number of blood cells and bacteria.

3.5. Detection of RBD of SARS-CoV-2 spike glycoprotein

For the evaluation of the sensing performance, a series of target RBD concentrations were measured with DPV under optimal conditions (Fig. S9†). Fig. 5A and S10† show the electrochemical responses of the biosensor toward a range of concentrations of RBD (from 1.0 pg mL^{-1} to 100.0 ng mL^{-1}). The linear fit function was $-\Delta I$ (μA) = 5.43 lg(C) + 67.92, with the linear correlation coefficient R^2 = 0.9958, and the calculated detection limit was 0.45 pg mL^{-1} (Fig. 5B). The experimental results also showed that the biosensor possessed a low detection limit and wide linear range for the COVID-19 antigen assay (Table S1†).[43–47]

3.6. Selectivity, stability, and reproducibility of the biosensor

The selectivity of the biosensor was evaluated by measurements of the target RBD and various potential interfering proteins including immunoglobulin G (IgG), immunoglobulin M (IgM), human epidermal growth factor receptor 2 (HER2), carbohydrate antigen 15-3 (CA15-3), carbohydrate antigen 12-5 (CA12-5), carcinoembryonic antigen (CEA), and alpha fetoprotein (AFP) (Fig. S11†). The biosensor exhibited great selectivity for the target RBD, while it displayed no significant responses to the interfering proteins even with higher concentrations.

Subsequently, to investigate the stability of the biosensor, the electrochemical signals before and after the detection of the target were evaluated by continuous DPV and CV tests in 5.0 mM $[Fe(CN)_6]^{3-/4-}$ solution. As shown in Fig. S12A,† the electrochemical signals before and after the RBD detection maintained good stability, with relative standard deviations (RSD) of 0.22% and 0.16%, respectively, for seven consecutive DPV scans. The stability is similarly illustrated by fifty CV scans in Fig. S12B.†

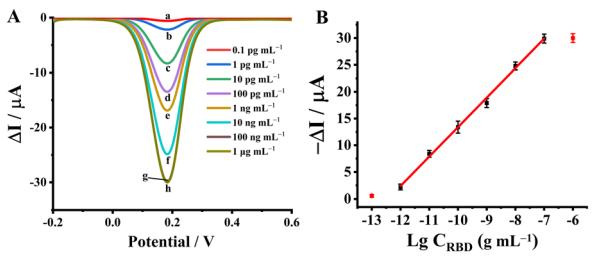

Fig. 5 (A) DPV responses of the electrochemical biosensor recorded at different concentrations of RBD after background subtraction. Curves (a–h) corresponding to RBD concentrations from 0.1 pg mL^{-1} to 1.0 μg mL^{-1}. (B) Linear calibration curve of the biosensor for RBD detection.

Additionally, the reproducibility of the biosensor was briefly evaluated, using seven batches of biosensors to assay RBD with the same concentration, and the measured signal responses exhibited an RSD of 2.68% (Fig. S13†). The result indicated the favorable reproducibility of the cyclic peptide-based biosensor.

3.7. Analysis of RBD in actual clinical samples

To assess the practical application potential of the biosensor for the assay of RBD in actual samples, 25% human blood samples spiked with different concentrations of RBD were detected (Fig. S14†), and the regression equation was $-\Delta I$ (μA) = 5.35 lg(C) + 67.13 (R^2 = 0.9956, detection limit of 0.47 pg mL^{-1}), which is in agreement with that in standard PBS, demonstrating that the sensing performance of the biosensor is not significantly affected by complex biological media.[48–50]

In addition, six human blood samples were collected from healthy volunteers and spiked with 0.1 ng mL^{-1}, 1.0 ng mL^{-1}, and 10.0 ng mL^{-1} RBD, respectively, and the RBD concentrations were measured with the biosensor and an ELISA kit. Fig. 6 shows that the recovery rates of the biosensor (red histograms) were remarkably favorable (95.1–99.4%), indicating that the biosensor can successfully capture and detect RBD with high accuracy; for the complex blood, the recovery rates of the ELISA kit were just 71.4–84.7% in 25% human blood. These results indicated that the biosensor was potentially more reliable than the ELISA kit for RBD detection in complex human blood.

Conclusions

In conclusion, an electrochemical biosensor was prepared based on a designed cyclic peptide for the specific detection of the SARS-CoV-2 spike glycoprotein RBD. The biosensor

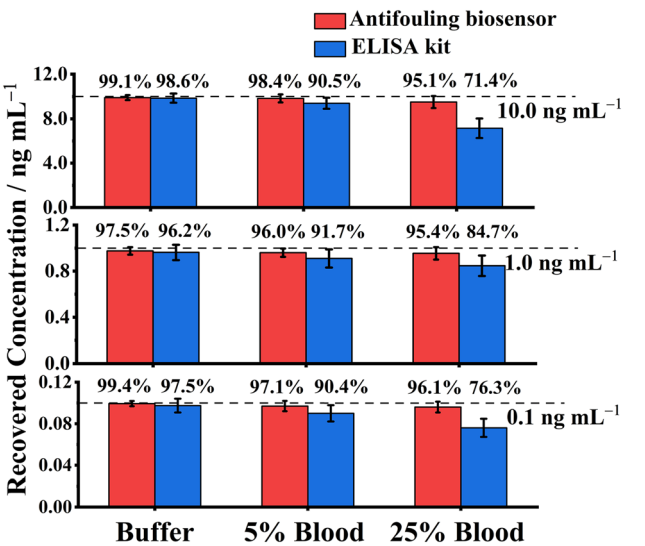

Fig. 6 Detection of RBD (0.1, 1.0, and 10.0 ng mL^{-1}) spiked in PBS and human blood (5% and 25%) with the biosensor (red) and an ELISA kit (blue). Data represent the mean recoveries across three repeated measurements.

exhibited noticeable resistance to biofouling and enzymatic hydrolysis even in human blood, due to the stable structure and the absence of amino acid terminals of the designed cyclic peptide. In addition, this biosensor showed good resistance to bacteria and blood cell adhesion, as well as long-term stability. More importantly, the biosensor enabled the accurate identification of RBD in complex human blood, and its performance was superior to that of an ELISA kit. This work offers a new perspective for early and direct detection of novel coronavirus antigens and is expected to be clinically applicable for SARS-CoV-2 screening.

Author contributions

Conceptualization: R. H. and X. L. Methodology: R. H. and X. L. Investigation: R. H., W. H., and X. L. Visualization: R. H. and Y. L. acquisition: R. H., M. C., C. D. and X. L. Supervision: R. H., M. C., C. D., and X. L. Writing – original draft: R. H. and Y. L. Writing – review & editing: R. H., C. D. and X. L.

Conflicts of interest

There are no conflicts to declare.

Acknowledgements

This work is supported by the National Natural Science Foundation of China (21974075, 22174082), the Taishan Scholar Program of Shandong Province of China (ts20110829), the Key Research and Development Program of Shandong Province (2021ZDSYS30) and the Science and Technology Benefiting the People Project of Qingdao (20-3-4-53-nsh).

Notes and references

1 G. Völkel, A. Fürstberger, J. D. Schwab, S. D. Werle, N. Ikonomi, T. Gscheidmeier, J. M. Kraus, A. Groß, M. Holderried, J. Balig, F. Jobst, P. Kuhn, K. A. Kuhn, O. Kohlbacher, U. X. Kaisers, T. Seufferlein and H. A. Kestler, *J. Med. Internet Res.*, 2021, **23**, e27348.
2 F. Zhou, T. Yu, R. Du, G. Fan, Y. Liu, Z. Liu, J. Xiang, Y. Wang, B. Song, X. Gu, L. Guan, Y. Wei, H. Li, X. Wu, J. Xu, S. Tu, Y. Zhang, H. Chen and B. Cao, *Lancet*, 2020, **395**, 1054–1062.
3 T. Ai, Z. Yang, H. Hou, C. Zhan, C. Chen, W. Lv, Q. Tao, Z. Sun and L. Xia, *Radiology*, 2020, **296**, E32–E40.
4 J. Zhao, Q. Yuan, H. Wang, W. Liu, X. Liao, Y. Su, X. Wang, J. Yuan, T. Li, J. Li, S. Qian, C. Hong, F. Wang, Y. Liu, Z. Wang, Q. He, Z. Li, B. He, T. Zhang, Y. Fu, S. Ge, L. Liu, J. Zhang, N. Xia and Z. Zhang, *Clin. Infect. Dis.*, 2020, **71**, 2027–2034.
5 F. Xiang, X. Wang, X. He, Z. Peng, B. Yang, J. Zhang, Q. Zhou, H. Ye, Y. Ma, H. Li, X. Wei, P. Cai and W.-L. Ma, *Clin. Infect. Dis.*, 2020, **71**, 1930–1934.
6 Z. Li, Y. Yi, X. Luo, N. Xiong, Y. Liu, S. Li, R. Sun, Y. Wang, B. Hu, W. Chen, Y. Zhang, J. Wang, B. Huang, Y. Lin, J. Yang, W. Cai, X. Wang, J. Cheng, Z. Chen, K. Sun, W. Pan, Z. Zhan, L. Chen and F. Ye, *J. Med. Virol.*, 2020, **92**, 1518–1524.
7 Q.-X. Long, B.-Z. Liu, H.-J. Deng, G.-C. Wu, K. Deng, Y.-K. Chen, P. Liao, J.-F. Qiu, Y. Lin, X.-F. Cai, D.-Q. Wang, Y. Hu, J.-H. Ren, N. Tang, Y.-Y. Xu, L.-H. Yu, Z. Mo, F. Gong, X.-L. Zhang, W.-G. Tian, L. Hu, X.-X. Zhang, J.-L. Xiang, H.-X. Du, H.-W. Liu, C.-H. Lang, X.-H. Luo, S.-B. Wu, X.-P. Cui, Z. Zhou, M.-M. Zhu, J. Wang, C.-J. Xue, X.-F. Li, L. Wang, Z.-J. Li, K. Wang, C.-C. Niu, Q.-J. Yang, X.-J. Tang, Y. Zhang, X.-M. Liu, J.-J. Li, D.-C. Zhang, F. Zhang, P. Liu, J. Yuan, Q. Li, J.-L. Hu, J. Chen and A.-L. Huang, *Nat. Med.*, 2020, **26**, 845–848.
8 Z. Li, J. Lu, W. Wei, M. Tao, Z. Wang and Z. Dai, *Chem. Commun.*, 2022, **58**, 12418–12430.
9 C. Huang, T. Wen, F.-J. Shi, X.-Y. Zeng and Y.-J. Jiao, *ACS Omega*, 2020, **5**, 12550–12556.
10 C. Shen, Z. Wang, F. Zhao, Y. Yang, J. Li, J. Yuan, F. Wang, D. Li, M. Yang, L. Xing, J. Wei, H. Xiao, Y. Yang, J. Qu, L. Qing, L. Chen, Z. Xu, L. Peng, Y. Li, H. Zheng, F. Chen, K. Huang, Y. Jiang, D. Liu, Z. Zhang, Y. Liu and L. Liu, *JAMA*, 2020, **323**, 1582–1589.
11 S. Cajigas, D. Alzate, M. Fernández, C. Muskus and J. Orozco, *Talanta*, 2022, **245**, 123482.
12 V. Vásquez, M.-C. Navas, J. A. Jaimes and J. Orozco, *Anal. Chim. Acta*, 2022, **1205**, 339718.
13 H. Hou, J. Mao, Y. Han, F. Wu, M. Zhang, D. Wang, L. Mao and Y. Li, *Sci. China: Chem.*, 2019, **62**, 1720–1724.
14 Y. Xu, X. Wang, C. Ding and X. Luo, *ACS Appl. Mater. Interfaces*, 2021, **13**, 20388–20396.
15 C. Jiang, G. Wang, R. Hein, N. Liu, X. Luo and J. J. Davis, *Chem. Rev.*, 2020, **120**, 3852–3889.
16 Z. Wang, C. Huang, N. Sun and C. Deng, *Sci. China: Chem.*, 2021, **64**, 932–947.
17 Y. Li, R. Han, M. Chen, X. Yang, Y. Zhan, L. Wang and X. Luo, *Anal. Chem.*, 2021, **93**, 14351–14357.
18 Y. Xu, Z. Wang, C. Ding and X. Luo, *Sens. Actuators, B*, 2020, **322**, 128613.
19 M. Chen, R. Han, W. Wang, Y. Li and X. Luo, *Anal. Chem.*, 2021, **93**, 13555–13563.
20 R. Han, Y. Li, M. Chen, W. Li, C. Ding and X. Luo, *Anal. Chem.*, 2022, **94**, 2204–2211.
21 R. Han, G. Wang, Z. Xu, L. Zhang, Q. Li, Y. Han and X. Luo, *Biosens. Bioelectron.*, 2020, **164**, 112317.
22 A. K. Nowinski, F. Sun, A. D. White, A. J. Keefe and S. Jiang, *J. Am. Chem. Soc.*, 2012, **134**, 6000–6005.
23 D. Takahashi, T. Yano and T. Fukui, *Org. Lett.*, 2012, **14**, 4514–4517.
24 H. Huang, D. Ganguly, J. Chen and X. S. Sun, *J. Nanosci. Nanotechnol.*, 2015, **15**, 4470–4479.
25 M. van der Knaap, J. M. Otero, A. Llamas-Saiz, M. J. van Raaij, L. I. Lageveen, H. J. Busscher, G. M. Grotenbreg, G. A. van der Marel, H. S. Overkleeft and M. Overhand, *Tetrahedron*, 2012, **68**, 2391–2400.
26 J.-S. Zheng, H.-N. Chang, J. Shi and L. Liu, *Sci. China: Chem.*, 2012, **55**, 64–69.
27 M. Gredičak, M. Abramić and I. Jerić, *Amino Acids*, 2012, **43**, 2087–2100.

28 M. Murakami, S. Suzuki, Y. Itou, S. Kodani and K. Ishida, *J. Nat. Prod.*, 2000, **63**, 1280–1282.
29 T. M. Williams, R. Sable, S. Singh, M. G. H. Vicente and S. D. Jois, *Chem. Biol. Drug Des.*, 2018, **91**, 605–619.
30 S. J. Bogdanowich-Knipp, S. Chakrabarti, T. J. Siahaan, T. D. Williams and R. K. Dillman, *J. Pept. Res.*, 1999, **53**, 530–541.
31 Y. Liang, S. Tang and J. S. Zheng, *Prog. Chem.*, 2014, **26**, 1793.
32 P. G. Dougherty, A. Sahni and D. Pei, *Chem. Rev.*, 2019, **119**, 10241–10287.
33 A. A. Vinogradov, Y. Yin and H. Suga, *J. Am. Chem. Soc.*, 2019, **141**, 4167–4181.
34 B. Kohnke, C. Kutzner and H. Grubmüller, *J. Chem. Theory Comput.*, 2020, **16**, 6938–6949.
35 D. Van Der Spoel, E. Lindahl, B. Hess, G. Groenhof, A. E. Mark and H. J. C. Berendsen, *J. Comput. Chem.*, 2005, **26**, 1701–1718.
36 K. Lindorff-Larsen, S. Piana, K. Palmo, P. Maragakis, J. L. Klepeis, R. O. Dror and D. E. Shaw, *Proteins*, 2010, **78**, 1950–1958.
37 M. Sastry, C. Brown, G. Wagner and T. D. Clark, *J. Am. Chem. Soc.*, 2006, **128**, 10650–10651.
38 P. Nagpal, S. Jamal, H. Singh, W. Ali, S. Tanweer, R. Sharma, A. Grover and S. Grover, *Sci. Rep.*, 2020, **10**, 4413.
39 V. Stockhausen, G. Trippé-Allard, N. Van Quynh, J. Ghilane and J.-C. Lacroix, *J. Phys. Chem. C*, 2015, **119**, 19218–19227.
40 Y. Mei, K. Yu, J. C. Y. Lo, L. E. Takeuchi, N. Hadjesfandiari, H. Yazdani-Ahmadabadi, D. E. Brooks, D. Lange and J. N. Kizhakkedathu, *ACS Nano*, 2018, **12**, 11881–11891.
41 R. J. Soto, J. R. Hall, M. D. Brown, J. B. Taylor and M. H. Schoenfisch, *Anal. Chem.*, 2017, **89**, 276–299.
42 G. Wang, R. Han, Q. Li, Y. Han and X. Luo, *Anal. Chem.*, 2020, **92**, 7186–7193.
43 M. A. Ali, C. Hu, S. Jahan, B. Yuan, M. S. Saleh, E. Ju, S.-J. Gao and R. Panat, *Adv. Mater.*, 2021, **33**, 2006647.
44 D. Soto and J. Orozco, *Anal. Chim. Acta*, 2022, **1205**, 339739.
45 M. Amouzadeh Tabrizi, J. P. Fernández-Blázquez, D. M. Medina and P. Acedo, *Biosens. Bioelectron.*, 2022, **196**, 113729.
46 E. B. Aydın, M. Aydın and M. K. Sezgintürk, *Sens. Actuators, B*, 2021, **345**, 130355.
47 M. Mohammadi, D. Antoine, M. Vitt, J. M. Dickie, S. Sultana Jyoti, J. G. Wall, P. A. Johnson and K. E. Wawrousek, *Anal. Chim. Acta*, 2022, **1229**, 340290.
48 R. Zeng, M. Qiu, Q. Wan, Z. Huang, X. Liu, D. Tang and D. Knopp, *Anal. Chem.*, 2022, **94**, 15155–15161.
49 R. Zeng, H. Gong, Y. Li, Y. Li, W. Lin, D. Tang and D. Knopp, *Anal. Chem.*, 2022, **94**, 7442–7448.
50 Z. Yu, H. Gong, J. Xu, Y. Li, Y. Zeng, X. Liu and D. Tang, *Anal. Chem.*, 2022, **94**, 3418–3426.